Chinese Journal of Physics 73 (2021) 239–255

Contents lists available at ScienceDirect

Chinese Journal of Physics

journal homepage: www.sciencedirect.com/journal/chinese-journal-of-physics

Irreversibilities in a triple diffusive flow in various porous cavities

Zafar H. Khan [a], Waqar A. Khan [b], Mikhail A. Sheremet [c], Jiguo Tang [a,*], Licheng Sun [a,*]

[a] State Key Laboratory of Hydraulics and Mountain River Engineering, College of Water Resource and Hydropower, Sichuan University, Chengdu 610065, PR China
[b] Department of Mechanical Engineering, College of Engineering, Prince Mohammad Bin Fahd University, Al Khobar 31952, Saudi Arabia
[c] Laboratory on Convective Heat and Mass Transfer, Tomsk State University, Tomsk 634050, Russia

ARTICLE INFO

Keywords:
Entropy generation
Triple diffusion
Natural convection
Porous cavities of different shapes

ABSTRACT

Entropy generation minimization approach is a very good method allowing to analyze the engineering systems to exclude technical failure. The present study deals with computational analysis of triple diffusive flow, energy transference and entropy production in different porous cavities from square to triangular through trapezoidal shape. The formulated boundary-value problem has been worked out using the finite element technique and non-primitive variables. The developed computational code has been verified using numerical results of other researchers. Analysis of entropy production due to energy and mass transport, motion friction, and porous material has been performed for different chamber's shapes. Entropy generation analysis in chambers of various geometries under the triple-diffusive flow is a novelty of the present research, where different entropy production mechanisms have been scrutinized for one complex problem. It has been ascertained that average total entropy generation strength raises with buoyancy ratios, Lewis and Rayleigh numbers, but it has the minimum value for the square chamber in comparison with triangular and trapezoidal shapes. Moreover, obtained results characterize a neglecting influence of motion friction on the total entropy generation.

1. Introduction

Entropy generation analysis is an effective technique for an investigation of technical systems in order to exclude bottlenecks and increase the operating time. Initially the entropy generation minimization method was developed by Bejan [1–3]. Nowadays, there are many published papers concerning usage of this technique for various engineering apparatus and regions. It is well-known that porous materials are employed in practice due to extended heat transfer area that characterizes an opportunity of the energy transport enhancement [4–6]. Also, such media can be found in electronic devices [7], solar power systems [8], heat exchangers [9,10], in human organism [11].

Technical analysis of heat and mass transfer in engineering devices including porous media is attended by entropy generation study [6,12–19]. Thus, Alsabery et al. [12] have numerically studied entropy production and convective energy transference in a porous wavy chamber under the influence of internal rotating cylinder. Using the finite element technique, authors have found that a rise of the medium porosity characterizes a reduction of the Bejan number. Moreover, the Bejan number can be decreased with a growth of the internal cylinder angular velocity. Biswal et al. [13] have simulated numerically the thermal convection and entropy production in

* Corresponding authors.
E-mail addresses: tangjiguo@sina.cn (J. Tang), sunlicheng@scu.edu.cn (L. Sun).

https://doi.org/10.1016/j.cjph.2021.06.017
Received 21 January 2021; Received in revised form 20 June 2021; Accepted 23 June 2021
Available online 23 July 2021

Nomenclature

Be_m	solute Bejan number
Be	Bejan number
c_p	heat capacity (J K^{-1})
C_m	concentration of solutes (kg m^{-3})
D_m	mass diffusivity of solutes S_m (m^2 s^{-1})
Da	Darcy number
$\mathbf{g}$	acceleration due to gravity (m s^{-2})
k	thermal conductivity of fluid (W m^{-1} K^{-1})
K	permeability of the porous medium (m^2)
Le_1	Lewis number of solute 1
Le_2	Lewis number of solute 2
Nc_1	dimensionless buoyancy parameter of solute 1
Nc_2	dimensionless buoyancy parameter of solute 2
N_S	local entropy generation rate
p	pressure (N m^{-2})
Q_0	dimensional internal heat generation/absorption coefficient
Q	non-dimensional internal heat generation
Ra	Rayleigh number
S_m	chemical components (“salts”)
T	fluid temperature (K)
T_0	$(T_h + T_c)/2$ (K)
$\mathbf{v}$	velocity vector
u, v	velocity components along x and y axes (m s^{-1})
x, y	Cartesian coordinates (m)

Greek letters

α_{pm}	thermal diffusivity of the porous medium (m^2 s^{-1})
β_T	coefficient of thermal expansion (K^{-1})
β_1, β_2	coefficient of thermal expansion of solute S_m (kg^{-1} m^3)
ΔC_1	concentration difference of salt 1 (kg m^{-3})
ΔC_2	concentration difference of salt 2 (kg m^{-3})
ε	porosity of the medium
χ_1	dimensionless concentration of solute 1
χ_2	dimensionless concentration of solute 2
ΔT	temperature difference (K)
μ	dynamic viscosity (N m^{-2} s)
ν	kinematic viscosity (m^2 s^{-1})
θ	dimensionless temperature
ρ	density (kg m^3)
ψ	stream function (m^2 s^{-1})
Φ	irreversibility ratio
Ω_T	dimensionless temperature difference ratio
Ω_{C1}	dimensionless concentration difference ratio due to salt 1
Ω_{C2}	dimensionless concentration difference ratio due to salt 2
$\Omega_{C1,2}$	dimensionless concentration difference ratio due to salt 1 & 2 coupling

Subscripts

c	cold
f	fluid
h	hot
$m = 1,2$	salt and concentration identifier
1, 2	due to coupling of salt 1 & 2

a tilted porous chamber using various thermal boundary conditions. Employing the Galerkin finite element technique authors have ascertained that the total entropy production owing to energy transference and liquid friction rises with modified Darcy and Prandtl numbers. An influence of local isothermal heaters on entropy production in a square porous cabinet has been scrutinized computationally by Kaluri and Basak [14]. It has been revealed that low Darcy number illustrates a domination of entropy production owing to the energy transference because of low medium permeability. At the same time, various arrangement of heaters illustrates different

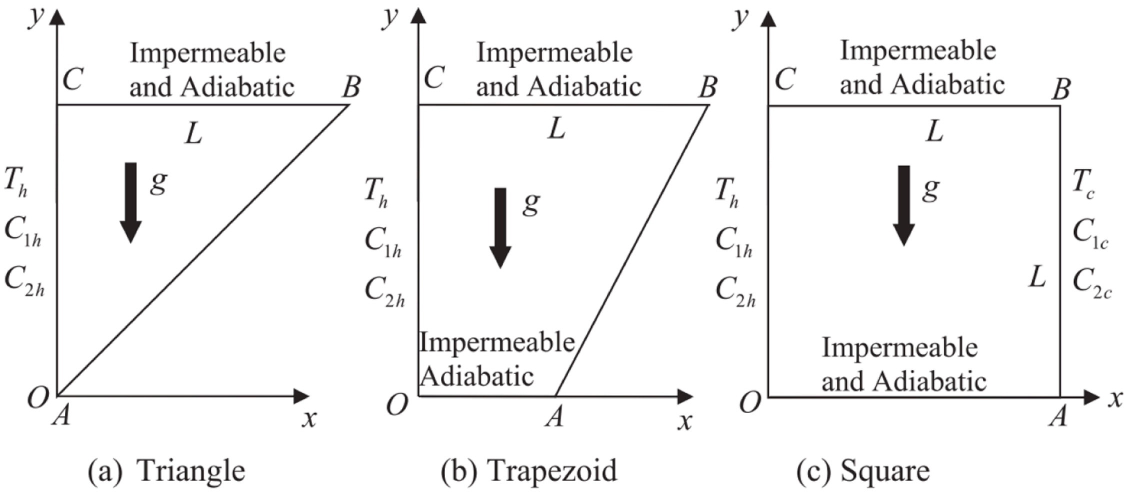

Fig. 1. Schematics of porous cavities[47].

entropy generation strength. Entropy generation in a porous trapezoidal [15] and triangular [16] cavities has been scrutinized using the Galerkin finite element method. Authors have demonstrated an influence of the cavity geometry on entropy production and found effective shapes with high energy transport strength and optimal entropy production. Baytas [17] has numerically investigated thermal convective energy transference and entropy production in a tilted square chamber. High Bejan number and low total entropy production have been found in the case of tilted chamber for high values of the inclination angle. Forced convection combined with entropy production in a rectangular channel with heated portions on the bottom and upper walls under the impacts of semi-porous fins has been scrutinized by Vatanparast et al. [18]. Authors have analyzed an influence of the Reynolds and Darcy numbers, thermal conductivity ratio, and size of fins on entropy generation intensity. As a result, optimal parameters have been found with minimal entropy production strength. Rashad et al. [19] have studied numerically natural convection of copper/water nanofluid in an inclined porous cavity under an influence of uniform magnetic field and local heater/cooler. It has been found that a rise of the nanoparticles concentration leads to the heat transfer degradation and average total entropy generation. Other interesting and useful results on thermal convection and entropy generation can be found in [20–27].

It should be noted that combined convective energy and mass transport within porous cabinets can be found in chemical engineering apparatus, solar collectors and other devices [28–32]. Thus, Arpino et al. [28] have developed an efficient artificial compressibility characteristic-based split technique for numerical simulation of transport phenomena in partially porous regions for forced, mixed and natural convection modes. It has been shown that this developed algorithm has a successful application for the studied class of phenomena. Baytas et al. [29] have examined numerically natural convective heat and mass transfer in a square cabinet partially filled with a porous material using local thermal equilibrium approach. Authors have revealed that porous steps have a critical influence of natural convection within the region. Massarotti et al. [30] have investigated numerically free convection in a partially porous gap between two tall cylinders under an impact of constant temperatures from internal and external cylinders. Authors have demonstrated that the porous insertion affects the transient temperature and velocity patterns, namely, fluctuations of temperature and velocity can be reduced for low Darcy numbers. Prasad et al. [31] using the finite element method have studied an influence of Soret and Dufour diffusion on unsteady MHD mixed convection of Casson liquid along the vertical wavy surface in a Darcy porous medium. It has been ascertained that an inclusion of Dufour and Soret effects allows to increase the velocity and temperature. He et al. [32] have examined numerically double-diffusive natural convection in a differentially heated and salted porous square chamber under an influence of temperature-dependent viscosity. Authors have shown that a diminution of viscosity with temperature affects the heat and mass transport strengths in the porous medium. Other useful outcomes can be found in [33–39].

At the same time, the mentioned complex analysis for combined convective energy and mass transport within porous cabinets is very important in the case of entropy generation investigation. Nowadays, there are several published papers on convective energy and mass transference in a chambers combined with entropy generation analysis [40–46]. Mchirgui et al. [40,41] have numerically studied double-diffusive thermal convection in a tilted porous enclosure using Darcy-Brinkman formulation with local thermal equilibrium approach. Authors have investigated an influence of the cavity inclination angle on entropy generation intensity. Effective values of all governing parameters have been found. Kefayati [42,43] has examined computationally thermal convection and entropy generation in a tilted porous chamber filled with non-Newtonian power-law liquid. Using the lattice Boltzmann technique, author has shown that the power-law index has a non-monotonic influence on the entropy generation intensity. Siavashi et al. [44] have performed the computational analysis of double-diffusive thermal convection and entropy production in a tilted porous chamber with internal isothermal heaters. Employing the finite volume method, authors have investigated the entropy generation strength behavior with several governing parameters. Authors have defined the optimal configuration with high heat and mass transport rates and low entropy production intensity. Zhu et al. [45] have computationally investigated 3D double-diffusion convection and entropy production in a porous cube filled with power-law liquid. They have demonstrated that the shear-thinning liquid is more effective in the case of energy and mass transference and entropy generation for double-diffusive convection.

This conducted brief review shows that combination of energy and mass transport with entropy generation analysis is a very topical. At the same time, there are no papers on triple-diffusive convection and entropy generation in chambers of various shapes. The objective of the present study is a computational investigation of triple-diffusive thermal convection and entropy production in a porous cabinet of different shapes. It should be noted that the present research is an expansion of the previous published paper [47] to the case of entropy generation analysis.

2. Governing equations for triple diffusion

The transport processes in various porous cavities presented in Fig. 1 are studied. The left sidewall is kept at a higher temperature T_h whereas as the right side/inclined wall is held at low temperature T_c ($< T_h$). Horizontal walls are adiabatic. A temperature dependent heat generation in the flow region has also been considered. Mathematical analysis of the examined phenomena is performed taking into account the following assumptions for fluid flow, heat and mass transfer

- steady triple-diffusive flow;
- two-dimensional case;
- laminar mode;
- walls of the cavities are impermeable;
- Boussinesq approximation is valid;
- linear Darcy law for the porous medium.

For the benefit of the reader, here, we will recall the main governing equations and boundary conditions.

Two different chemical components ("salts") S_m ($m = 1{,}2$) have been dissolved in a fluid-saturated porous medium, which have concentrations C_m ($m = 1{,}2$), respectively, and that the equation of state is [48]

$$\rho = \rho_0 [1 - \beta_T \Delta T + \beta_1 \Delta C_1 + \beta_2 \Delta C_2] \tag{1}$$

where $\Delta T = T - T_0$, $\Delta C_1 = C_1 - C_{1C}$, and $\Delta C_2 = C_2 - C_{2C}$. The reference density, temperature and salt concentrations are denoted by ρ_0, T_0, C_{1C} and C_{2C}, respectively, while the constants β_T, β_1 and β_2 denote the coefficient of thermal expansion and solute S_m expansion coefficients, respectively ($m = 1{,}2$), which are defined by Rionero [48]

$$\beta_T = -\frac{1}{\rho}\left(\frac{\partial \rho}{\partial T}\right)_p, \quad \beta_1 = -\frac{1}{\rho}\left(\frac{\partial \rho}{\partial C_1}\right)_p, \quad \beta_2 = -\frac{1}{\rho}\left(\frac{\partial \rho}{\partial C_2}\right)_P \tag{2}$$

Combining Darcy's law [49]

$$\frac{\mu}{K}\mathbf{v} = -\nabla p + \rho \mathbf{g} \tag{3}$$

with (thermal) energy and mass balance together with the Boussinesq approximation (1), we obtain the following fundamental equations governing the isochoric motions [47–49]

$$\nabla \cdot \mathbf{v} = 0 \tag{4}$$

$$\frac{\mu}{K}\mathbf{v} = -\nabla p + \rho_0 [1 - \beta_T \Delta T + \beta_1 \Delta C_1 + \beta_2 \Delta C_2]\,\mathbf{g} \tag{5}$$

$$\mathbf{v} \cdot \nabla T = \alpha_{pm} \nabla^2 T + \frac{Q_0}{\rho c_p}(T - T_c) \tag{6}$$

$$\frac{1}{\varepsilon}\mathbf{v} \cdot \nabla C_1 = D_1 \nabla^2 C_1 \tag{7}$$

$$\frac{1}{\varepsilon}\mathbf{v} \cdot \nabla C_2 = D_2 \nabla^2 C_2 \tag{8}$$

where $\mathbf{v}$ is the velocity vector, p is the pressure field, μ is the dynamic viscosity, K is the permeability, $\mathbf{g}$ is the gravity vector, α_{pm} is the thermal diffusivity of the porous medium and D_m ($m = 1{,}2$) are the mass diffusivity of the solute S_m.

The appropriate boundary conditions are [47]

(i) For the horizontal top and bottom walls OA and BC, $u = v = \frac{\partial T}{\partial y} = \frac{\partial C_1}{\partial y} = \frac{\partial C_2}{\partial y} = 0$ (9)
(ii) For the left-side wall OC, $u = v = 0, T = T_h, C_1 = C_{1h}, C_2 = C_{2h}$ (10)
(iii) For the right-side wall AB, $u = v = 0, T = T_c, C_1 = C_{1c}, C_2 = C_{2c}$(11)

To write the governing equations and boundary conditions (4)–(11) in a non-dimensional form, we employ the following parameters along with the dimensionless stream function:

$$X=\frac{x}{L},Y=\frac{y}{L},u=\frac{\alpha_{pm}}{L}U,v=\frac{\alpha_{pm}}{L}V,T=(T_h-T_c)\theta+T_c,Q=\frac{Q_0L^2}{\alpha_{pm}\rho c_p}$$
$$C_1=(C_{1h}-C_{1c})\chi_1+C_{1c},C_2=(C_{2h}-C_{2c})\chi_2+C_{2c},U=\frac{\partial\psi}{\partial Y},V=-\frac{\partial\psi}{\partial X} \tag{12}$$
$$Ra=\frac{gK\beta_T\Delta TL}{\upsilon\alpha_{pm}},Nc_1=\frac{\beta_1\Delta C_1}{\beta_T\Delta T},Nc_2=\frac{\beta_2\Delta C_2}{\beta_T\Delta T},Le_1=\frac{\alpha_{pm}}{\varepsilon D_1},Le_2=\frac{\alpha_{pm}}{\varepsilon D_2}$$

Using Eq. (12), Eqs. (4)–(8) can be transformed to the non-dimensional form

$$\frac{\partial^2\Psi}{\partial X^2}+\frac{\partial^2\Psi}{\partial Y^2}=-Ra\left(\frac{\partial\theta}{\partial X}+Nc_1\frac{\partial\chi_1}{\partial X}+Nc_2\frac{\partial\chi_2}{\partial X}\right) \tag{13}$$

$$\frac{\partial\Psi}{\partial Y}\frac{\partial\theta}{\partial X}-\frac{\partial\Psi}{\partial X}\frac{\partial\theta}{\partial Y}=\frac{\partial^2\theta}{\partial X^2}+\frac{\partial^2\theta}{\partial y^2}+Q\theta \tag{14}$$

$$\frac{\partial\Psi}{\partial Y}\frac{\partial\chi_1}{\partial X}-\frac{\partial\Psi}{\partial X}\frac{\partial\chi_1}{\partial Y}=\frac{1}{Le_1}\left(\frac{\partial^2\chi_1}{\partial X^2}+\frac{\partial^2\chi_1}{\partial Y^2}\right) \tag{15}$$

$$\frac{\partial\Psi}{\partial Y}\frac{\partial\chi_2}{\partial X}-\frac{\partial\Psi}{\partial X}\frac{\partial\chi_2}{\partial Y}=\frac{1}{Le_2}\left(\frac{\partial^2\chi_2}{\partial X^2}+\frac{\partial^2\chi_2}{\partial Y^2}\right) \tag{16}$$

The additional non-dimensional conditions are

(i) For the horizontal top and bottom borders, $\Psi=\frac{\partial\theta}{\partial Y}=\frac{\partial\chi_1}{\partial Y}=\frac{\partial\chi_2}{\partial Y}=0$ (17)
(ii) For the left sidewall, $\Psi=0,\theta=1,\chi_1=1,\chi_2=1$ (18)
(iii) For the right sidewall, $\Psi=0,\theta=0,\chi_1=0,\chi_2=0$ (19)

3. Entropy generation model

In a triple-diffusive natural convection system of non-isothermal flows in porous media without chemical reactions, the associated sources of irreversibility are due to heat transfer, momentum transfer (fluid friction), porous medium (pm), mass transfer of salts concentrations C_1 and C_2, and the coupling between salts concentrations C_1 and C_2. The general expression for the entropy generation rate for triple diffusive flow in two dimensions can be written as [50]

$$\dot{S''}_{gen}=\frac{k_f}{T_0^2}\left[\left(\frac{\partial T}{\partial x}\right)^2+\left(\frac{\partial T}{\partial y}\right)^2\right]+\frac{\mu}{KT_0}\left(u^2+v^2\right)+\frac{\mu}{T_0}\left[2\left(\frac{\partial u}{\partial x}\right)^2+2\left(\frac{\partial v}{\partial y}\right)^2+\left(\frac{\partial u}{\partial x}+\frac{\partial v}{\partial y}\right)^2\right]$$
$$+\frac{RD_1}{C_0}\left[\left(\frac{\partial C_1}{\partial x}\right)^2+\left(\frac{\partial C_1}{\partial y}\right)^2\right]+\frac{RD_1}{T_0}\left[\frac{\partial C_1}{\partial x}\frac{\partial T}{\partial x}+\frac{\partial C_1}{\partial y}\frac{\partial T}{\partial y}\right]+\frac{RD_2}{C_0}\left[\left(\frac{\partial C_2}{\partial x}\right)^2+\left(\frac{\partial C_2}{\partial y}\right)^2\right] \tag{20}$$
$$+\frac{RD_2}{T_0}\left[\frac{\partial C_2}{\partial x}\frac{\partial T}{\partial x}+\frac{\partial C_2}{\partial y}\frac{\partial T}{\partial y}\right]+\frac{RD_{12}}{C_0}\left[\frac{\partial C_1}{\partial x}\frac{\partial C_2}{\partial x}+\frac{\partial C_1}{\partial y}\frac{\partial C_2}{\partial y}\right]$$

The dimensionless entropy generation rate N_S is defined as the ratio of the local volumetric entropy generation rate $\dot{S''}_{gen}$ to a characteristic entropy generation rate $\dot{S''}_{gen,0}=T_0^2L^2/(k_f\Delta T^2)$. Therefore, the dimensionless entropy generation rate is $N_S=\dot{S''}_{gen}/\dot{S''}_{gen,0}$. The non-dimensional form of local entropy generation rate is given as

$$N_S=\underbrace{\left\{\left(\frac{\partial\theta}{\partial X}\right)^2+\left(\frac{\partial\theta}{\partial Y}\right)^2\right\}}_{N_{S,h}}+\underbrace{\varphi_1\left[\left\{\left(\frac{\partial\psi}{\partial X}\right)^2+\left(\frac{\partial\psi}{\partial Y}\right)^2\right\}+Da\left\{4\left(\frac{\partial^2\psi}{\partial X\partial Y}\right)^2+\left(\frac{\partial^2\psi}{\partial Y^2}-\frac{\partial^2\psi}{\partial X^2}\right)^2\right\}\right]}_{N_{S,pm}+N_{S,f}}$$
$$+\underbrace{\varphi_2\left[\frac{\Omega_{C_1}}{\Omega_T}\left\{\left(\frac{\partial\chi_1}{\partial X}\right)^2+\left(\frac{\partial\chi_1}{\partial Y}\right)^2\right\}+\left\{\frac{\partial\chi_1}{\partial X}\frac{\partial\theta}{\partial X}+\frac{\partial\chi_1}{\partial Y}\frac{\partial\theta}{\partial Y}\right\}\right]}_{N_{S,C_1}} \tag{21}$$
$$+\underbrace{\varphi_3\left[\frac{\Omega_{C_2}}{\Omega_T}\left\{\left(\frac{\partial\chi_2}{\partial X}\right)^2+\left(\frac{\partial\chi_2}{\partial Y}\right)^2\right\}+\left\{\frac{\partial\chi_2}{\partial X}\frac{\partial\theta}{\partial X}+\frac{\partial\chi_2}{\partial Y}\frac{\partial\theta}{\partial Y}\right\}\right]}_{N_{S,C_2}}+\underbrace{\varphi_4\left\{\frac{\partial\chi_2}{\partial X}\frac{\partial\theta}{\partial X}+\frac{\partial\chi_2}{\partial Y}\frac{\partial\theta}{\partial Y}\right\}}_{N_{S,C_{12}}}$$

In the above equation, the dimensionless parameters are defined as:

$$\Omega_T = \frac{\Delta T}{T_0}, B = \frac{\mu\alpha_m^2}{k_f T_0 L^2}, Da = \frac{K}{L^2}, \Omega_{C_1} = \frac{\Delta C_1}{C_0}, \Omega_{C_2} = \frac{\Delta C_2}{C_0},$$
$$M_1 = \frac{RD_1C_0}{k_f}, M_2 = \frac{RD_2C_0}{k_f}, M_3 = \frac{RD_{12}C_0}{k_f}, \varphi_1 = \frac{B}{\Omega_T^2 Da}, \varphi_2 = \frac{M_1\Omega_{C_1}}{\Omega_T}, \varphi_3 = \frac{M_2\Omega_{C_2}}{\Omega_T}, \varphi_4 = \frac{M_3\Omega_{C_1}\Omega_{C_2}}{\Omega_T^2} \tag{22}$$

3.1. Entropy generation number

The entropy generation number can be obtained by integrating the local entropy generation rate over the whole domain of the cavity volume as

$$N_{S,avg} = \int_\Omega N_S \partial\Omega \tag{23}$$

where Ω represents the global computational domain and N_S is the total entropy generation rate in triple diffusion, given by

$$N_S = N_{S,h} + N_{S,pm} + N_{S,f} + N_{S,C_1} + N_{S,C_2} + N_{S,C_{12}} = N_{S,h} + N_{\mathrm{S,othersources}}$$

3.2. Irreversibility ratio

The local irreversibility Φ is defined as a ratio between the local entropy generation rate due to fluid friction to the local entropy generation rate due to heat transfer $N_{S,h}$

$$\Phi = \frac{N_{S,f}}{N_{S,h}} \tag{24}$$

It is essential to mention that when $\Phi > 1$ then irreversibility due to fluid friction is the dominated factor, whereas when $0 < \Phi < 1$ the heat transfer irreversibility dominants.

The average dimensionless irreversibility ratio is obtained by numerical integration of the local dimensionless ratio over the entire cavity volume and is given by

$$\Phi_{avg} = \int_\Omega \Phi \partial\Omega \tag{25}$$

3.3. Heat Bejan number

The conventional local Bejan number is the ratio between the local entropy generation rate due to heat transfer $N_{S,h}$ to the total entropy generation rate N_S, the relation that describes this number is expressed as

$$Be_h = \frac{N_{S,h}}{N_S} = \frac{N_{S,h}}{N_{S,h} + N_{\mathrm{S,othersources}}} = \frac{1}{1 + \frac{N_{\mathrm{S,othersources}}}{N_{S,h}}}$$
$$\text{where} N_{\mathrm{s,othersources}} = N_{s,pm} + N_{s,f} + N_{s,C_1} + N_{s,C_2} + N_{s,C_{12}} \tag{26}$$

It is important to note that

(i) When the thermal irreversibility plays a major contribution $N_{S,h} \to \infty$, $Be_h = 1$.
(ii) When the other sources contribute dominant part in entropy generation$N_{S,h} \to 0$, $Be_h = 0$.
(iii) When both heat and other sources contribute equally, $Be_h = 0.5$.

The average dimensionless Bejan number due to heat transfer is obtained by numerical integration the local dimensionless one over the entire cavity volume and it is given by

$$Be_{h,avg} = \int_\Omega Be_h \partial\Omega \tag{27}$$

3.4. Mass Bejan number

A new type of mass local Bejan number is presented here, which is the ratio between the sum of local entropy generation rate due to mass transfer of salts concentrations C_1 and C_2, and the coupling between salts C_1 and C_2, i.e., $N_{S,C_1} + N_{S,C_2} + N_{S,C_{12}}$ to the total entropy generation N_S and is defined as

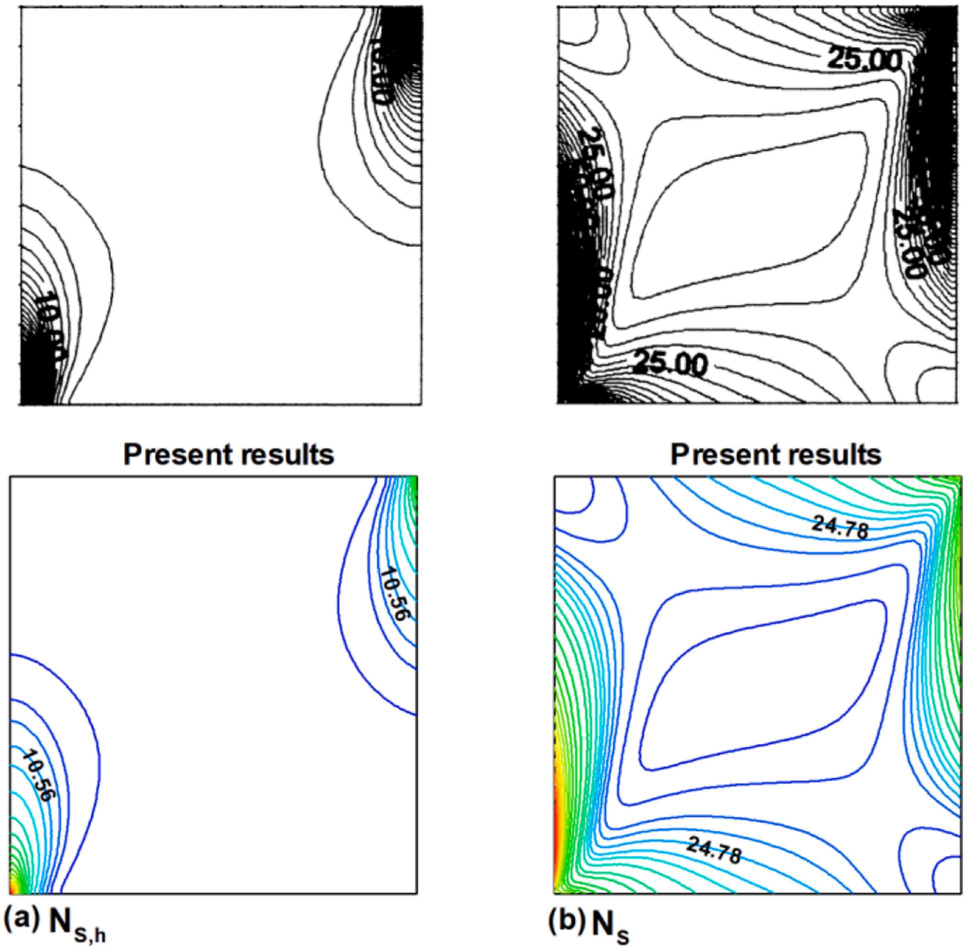

Fig. 2. Comparison of the results in a case of fluid without any salts with literature [17] for (a) entropy generation due to heat transfer ($N_{S,h}$) and (b) total entropy generation number (N_S) with $Ra = 100$ and $\phi_1 = 10^{-1}$.

$$Be_{mass} = \frac{N_{S,C}}{N_S} = \frac{N_{S,C}}{N_{S,C} + N_{\mathrm{S,othersources}}} = \frac{1}{1 + \frac{N_{\mathrm{S,othersources}}}{N_{S,C}}} \quad (28)$$

$$\text{where} N_{\mathrm{S,othersources}} = N_{S,h} + N_{S,pm} + N_{S,f} \text{and} N_{S,C} = N_{S,C_1} + N_{S,C_2} + N_{S,C_{12}}$$

where $N_{S,C}$ is the entropy generation due to solutes and their coupling.

It is important to note that

(i) When the solutal irreversibility plays a major contribution$N_{S,C} \to \infty$, $Be_{mass} = 1$.
(ii) When the other sources contribute dominant part in entropy generation $N_{S,C} \to 0$, $Be_{mass} = 0$.
(iii) When both solutes and other sources contribute equally, $Be_{mass} = 0.5$.

The average dimensionless mass Bejan number is obtained by numerical integration of the local one over the entire cavity volume and are given by

$$Be_{mass,avg} = \int_{\Omega} Be_{mass} \partial\Omega \quad (29)$$

where the symbol Ω represents the global computational domain.

4. Validation of results

We have already shown the reliability and accuracy of the method used to obtain the results in our previous paper [47]. To show the

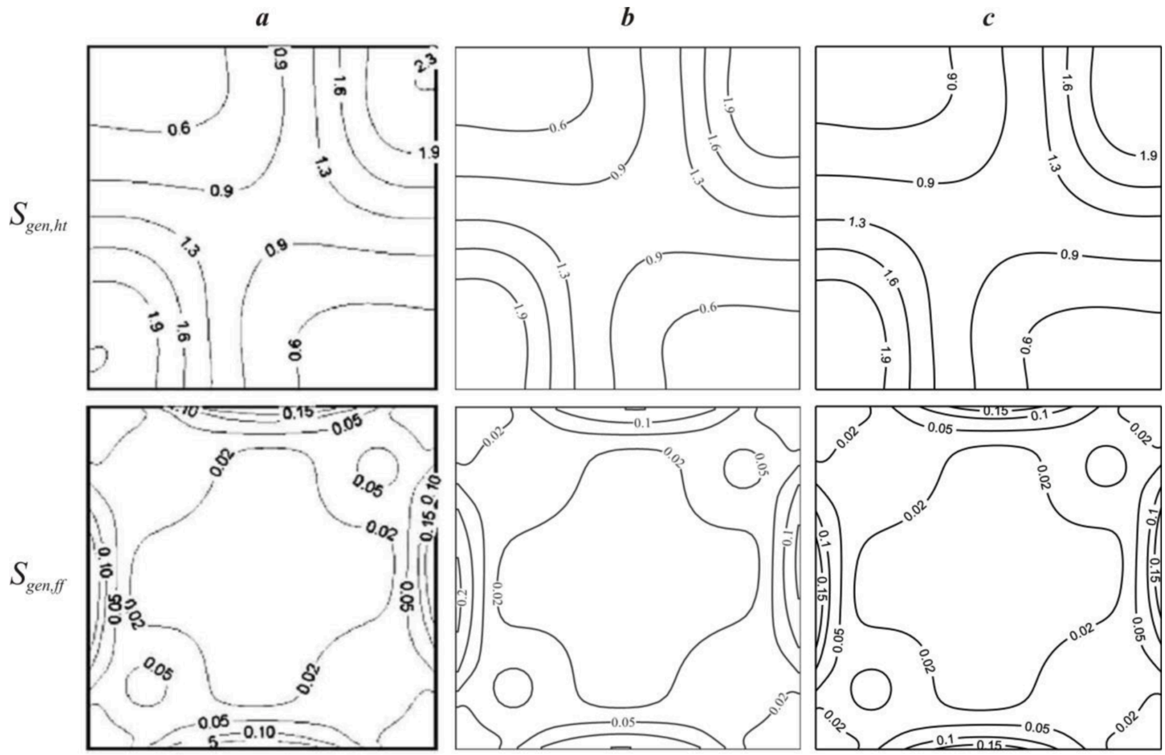

Fig. 3. Comparison of local entropy production owing to energy transport $S_{gen,ht}$ and liquid friction $S_{gen,ff}$ for $Ra = 10^3$: computational results [51] – *a*, computational results [52] – *b*, present results – *c*.

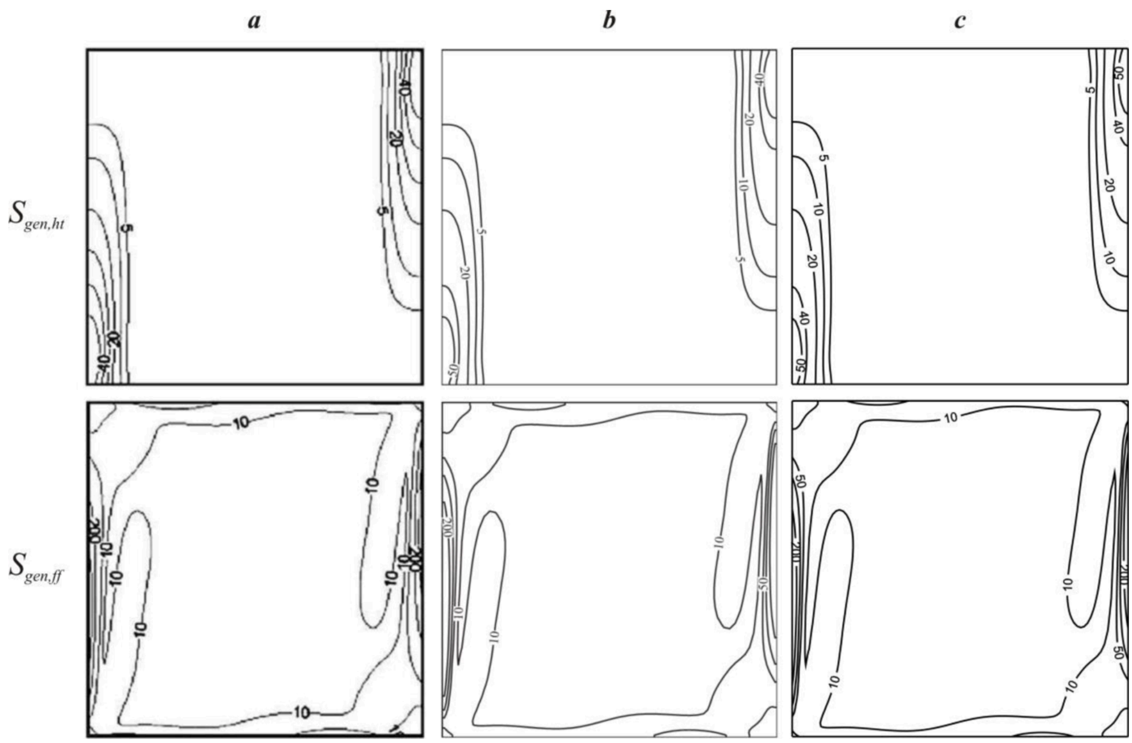

Fig. 4. Comparison of local entropy production owing to energy transport $S_{gen,ht}$ and liquid friction $S_{gen,ff}$ for $Ra = 10^5$: computational results [51] – *a*, computational results [52] – *b*, present results – *c*.

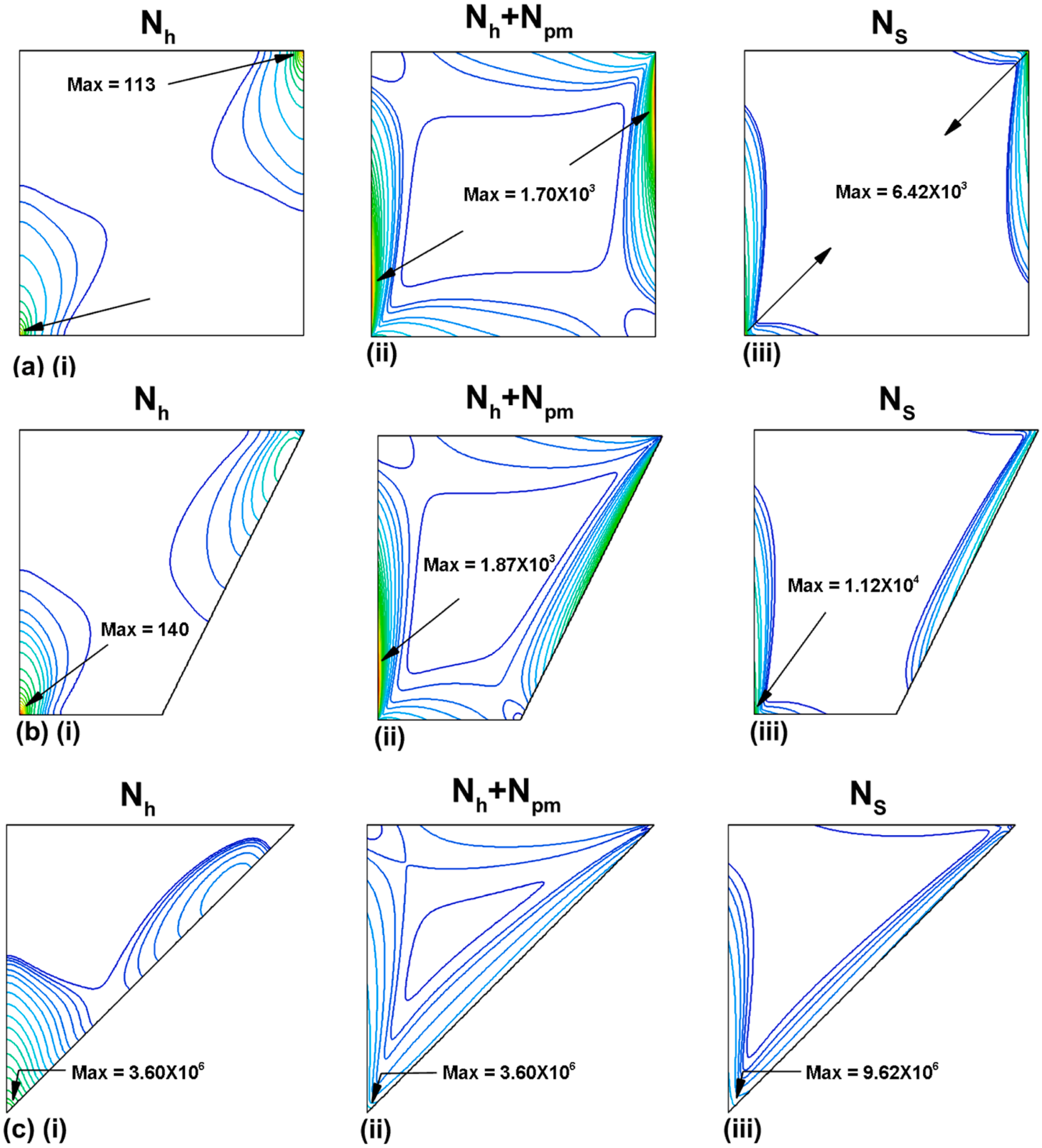

Fig. 5. Iso-contours of entropy generation due to (i) heat (ii) heat in porous media and (iii) triple diffusion in porous media in different cavities with $Ra = 50, Nc_1 = Nc_2 = 0.5, Le_1 = 8, Le_2 = 5, Q = 0.5, \varphi_1 = 0.5, Da = 10^{-4}, \varphi_2 = \varphi_3 = \varphi_4 = 0.5$.

validation of the proposed method, we have made comparison with the literature [17] for a special case of pure fluid flow in a porous square cavity. The results are presented in Fig. 2. for entropy generation due to heat transfer and total entropy generation rate and they are found to be in a good agreement with the literature.

The second test was thermal convection in a square chamber. Figs. 3 and 4 demonstrate a good agreement between the iso-contours of local entropy generation owing to energy transport and fluid friction for various Rayleigh numbers with the numerical results of Ilis et al. [51] and Bhardwaj et al. [52].

5. Results and discussion

The entropy generation due to several sources of irreversibility is investigated in the selected cavities. The dimensionless governing equations are solved numerically and the velocity, temperature, concentration gradients are utilized in the entropy generation model. The effects of governing parameters on the entropy generation due to various sources, Bejan numbers and irreversibility ratio are

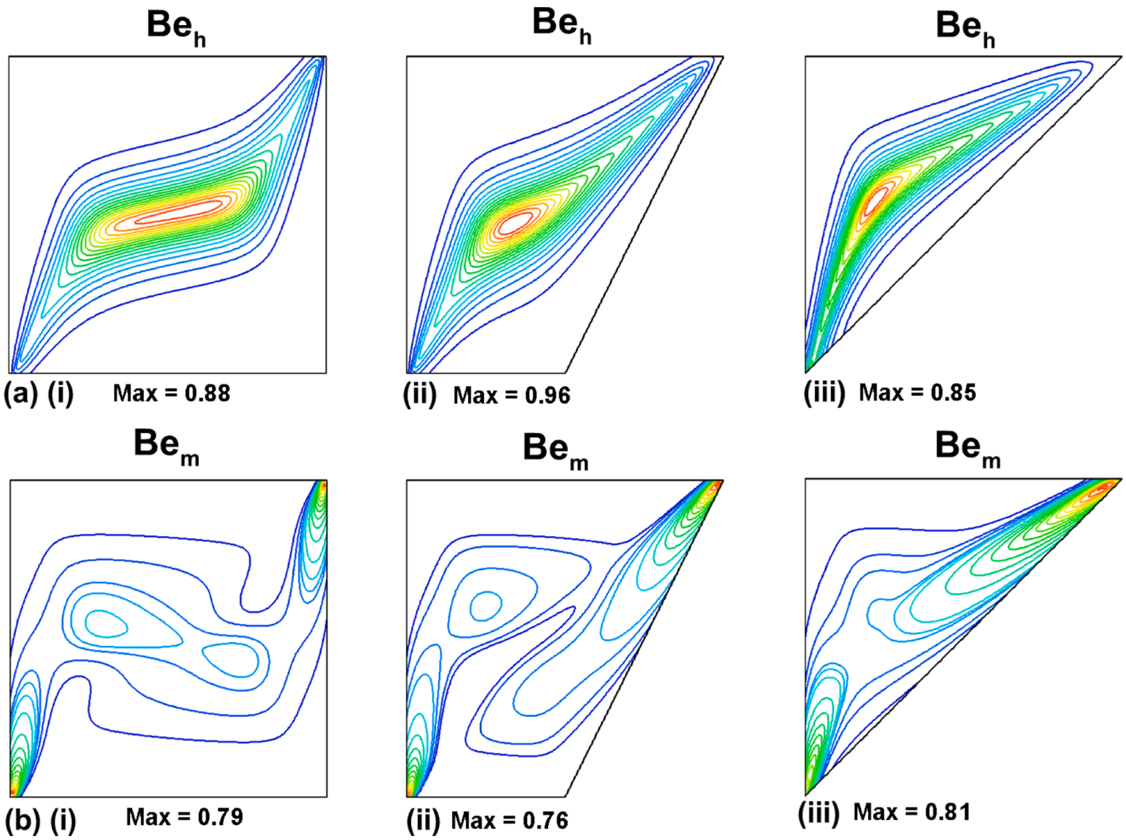

Fig. 6. Iso-Countors of (a) heat Bejan number and (b) mass Bejan number in different cavities with $Ra = 50, Nc_1 = Nc_2 = 0.5, Le_1 = 8, Le_2 = 5, Q = 0.5, \varphi_1 = 0.5, Da = 10^{-4}, \varphi_2 = \varphi_3 = \varphi_4 = 0.5$.

investigated and discussed.

The iso-contours of total entropy generation and its components due to heat transfer and porous medium are displayed in Fig. 5 in the selected cavities. The entropy generation due to thermal irreversibility ensues near the hot and cold regions, see Fig. 5(i). The iso-contours due to thermal and porous medium are produced in Fig. 5(ii). In each case, the maximum values of irreversibility pinpoint in the lower region close to the hot wall of the cavity. Local entropy generation is located in the upper corner of the cooled side and lower corner of the heated side of the cavity.

The iso-contours of local heat and mass Bejan numbers are displayed in Fig. 6(a) and (b) for low Rayleigh numbers in the selected cavities. It is well known that, for low Rayleigh numbers, the thermal irreversibility is muscularly leading and the heat Bejan number upsurges with an increase in the heat transfer. This is imitated in Fig. 6 (a) (i)–(iii), where the local $Be_h > 0.80$ in all cavities. These figures reveal that the thermal irreversibility is dominant over other sources. The value of Be_h is found to be highest in the trapezoidal cavity and lowest in the triangular cavity. The mass Bejan number measures the contribution of total irreversibility due to diffusion of species and their coupling $N_{S,C}$ in the cavity. The Fig. 6 (b) (i)–(iii) show the iso-contours of Be_m in the selected cavities. It is concluded that when $N_{S,C} \to \infty$, $Be_m \to 1$. In Fig. 6 (b) (iii), the maximum value of Be_m is noticed.

The variation of individual local components of entropy generation rate, Bejan numbers and irreversibility ratio along X-axis at the centers of each cavity is displayed in Fig. 7(a) and (b) for the fixed values of the pertinent parameters. It is important to note that the entropy generation due to the coupling of both species is maximum at the hot and cold walls in each cavity, Fig. 7(a) (i)–(iii). This is due to higher temperature and concentration gradients at the left and right walls. The second and third major sources of irreversibility are the porous medium and heat transfer. The entropy generation due to these sources is also maximum at the right and cold walls in each case. On the other side, the entropy generation rates due to friction and each solute are found to be minimum in each case. Fig. 7 (b) explains the variation of both Bejan numbers and irreversibility ratio along Y-axis at $X = 0.5$. The heat and mass Bejan numbers measure the contribution of thermal or solutal irreversibility in the total entropy generation. It is noticed that Be_h is minimum at the hot and cold walls and increases at the central position in each case. This is due to higher temperature gradients in the central region. The mass Bejan numbers show opposite behavior. They are higher at the walls and decrease in the central region. The irreversibility ratio shows the importance of irreversibility due to fluid friction and heat transfer. It is necessary to indicate here $\Phi < 1$ in each case, which shows that the thermal irreversibility is dominant over viscous irreversibility.

The contribution of the numerous sources of irreversibility in the total entropy generation rate along center position of each cavity is presented in Fig. 8. The main sources of irreversibility include heat and mass transfer, fluid friction, porous medium and magnetic

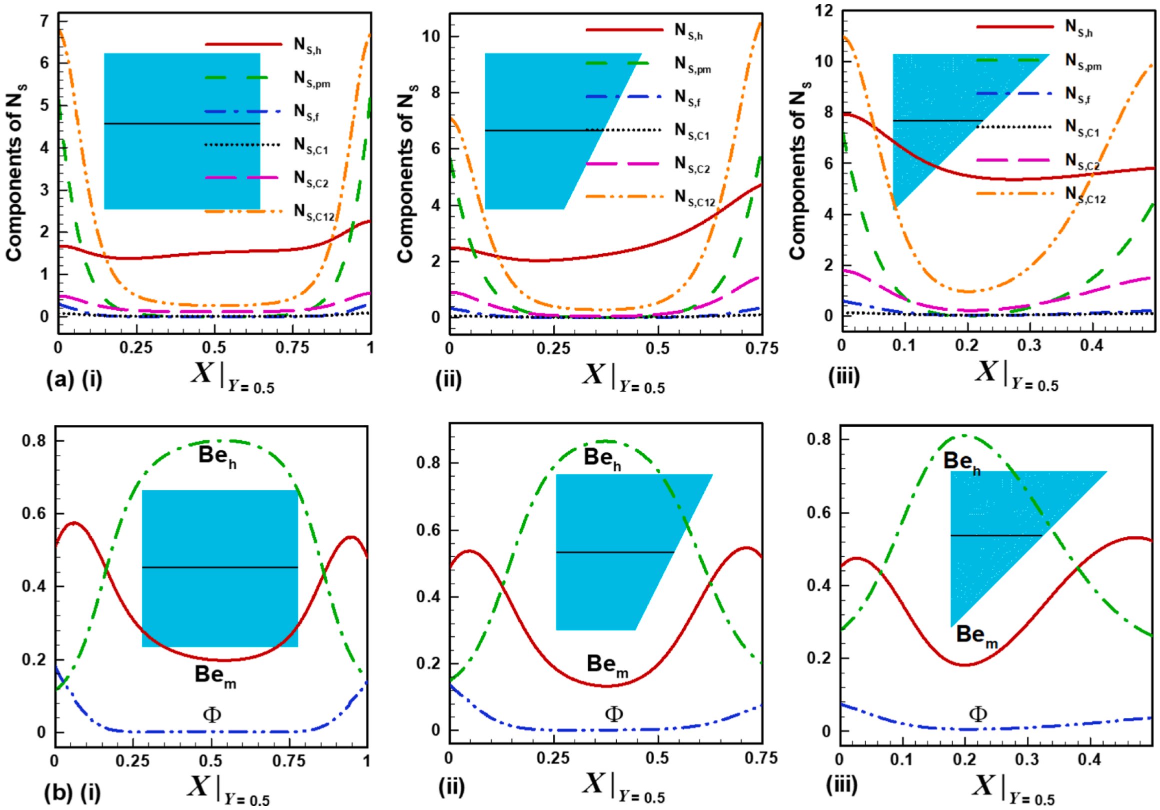

Fig. 7. Variations in (a) different components of local entropy generation and (b) irreversibility ratio, heat and mass Bejan numbers for different cavities with $Q = Nc_1 = Nc_2 = \varphi_1 = \varphi_2 = \varphi_3 = \varphi_4 = 0.5$, $Ra = 50, Le_1 = 8, Le_2 = 5, Da = 10^{-4}$.

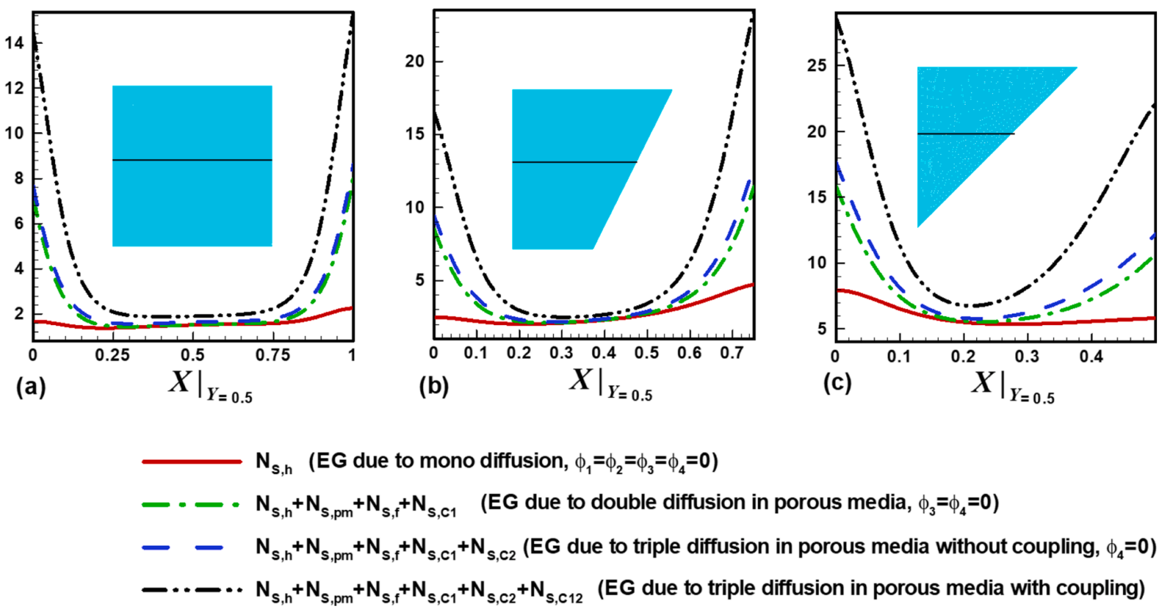

Fig. 8. Effects of diffusion on total local entropy generation in selected cavities with $Ra = 50, Le_1 = 8, Le_2 = 5, Da = 10^{-4}, \varphi_2 = 10^{-2}, \varphi_1 = \varphi_3 = 10^{-1}, Q = Nc_1 = Nc_2 = \varphi_4 = 0.5$.

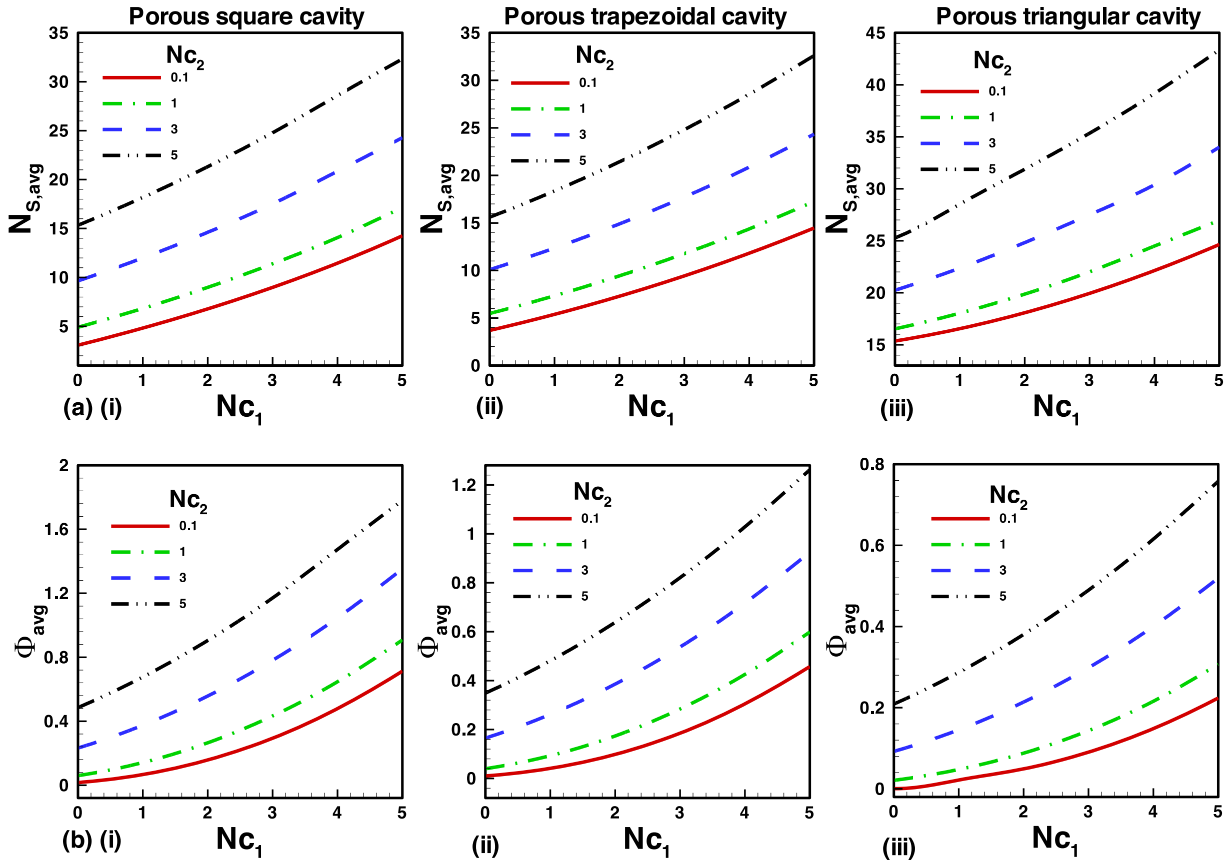

Fig. 9. Effects of buoyancy ratios on (a) average total entropy generation rate (b) average irreversibility ratio with $Ra = 50, Le_1 = 8, Le_2 = 5, Da = 10^{-4}, Q = \varphi_1 = \varphi_2 = \varphi_3 = \varphi_4 = 0.5$.

field. In the absence of all other sources, the variation of thermal irreversibility (mono diffusion) is found to be minimum in case of square cavity (Fig. 8a) and maximum in the triangular cavity (Fig. 8c). As expected, the irreversibility increases with the addition of other sources due to double and triple diffusion. The maximum irreversibility ensues at the hot and cold wall in each cavity for triple diffusion with coupling. In the central region of each cavity, the entropy generation rate is found to be minimum. The triple diffusion with/without coupling is basically exemplified by the combined heat and mass transfer associated the entropy generation.

The variation of the average total entropy generation rates and irreversibility ratios with buoyancy ratios are presented in Fig. 9(a) and (b) for the selected geometries. It is important to note that the average total entropy generation rate increases with an increase in each buoyancy ratio in each case. The buoyancy ratios depend upon the concentration difference ΔC which help in increasing the solutal irreversibility. Consequently, the total entropy generation rate increases. This is confirmed in Fig. 9(a) (i)–(iii) for each cavity. On the other side, the irreversibility ratio is directly proportional to the fluid flow irreversibility which in turn depends upon the ΔT. When ΔT decreases, the buoyancy ratios increase and as a result Φ_{avg} increases with both buoyancy ratios in each case (see Fig. 9(b) (i)–(iii)).

The combined effects of both solute Lewis numbers on the average entropy generation are displayed in Fig. 10(a) and the average irreversibility ratio in Fig. 10(b) for the selected cavities. The Lewis numbers play a vital role in the case of combined heat and mass transfer. It measures the comparative thermal and solutal resistances. It is important to note that, for smaller values of Le_1 and Le_2, the effects of each Lewis number on the average total entropy generation are negligible and become evident for higher values in each cavity. In each case, the Lewis number is greater than 1 which shows the superiority of the solutal boundary layer. As the Lewis numbers increase, the total solutal resistance increases and consequently the total average total entropy generation increases as shown in Fig. 10(a) (i)–(iii). The variation of average irreversibility ratio with Le_1 and Le_2 is depicted in Fig. 10(b) (i)–(iii) for the selected geometries. Like $N_{s,avg}$, the average irreversibility ratio increases with an increase in both Lewis numbers. The Lewis number depends upon the thermal diffusivity and measures the rate of heat transfer. The entropy generation rate due to heat transfer decreases with an increase in the Lewis number which helps in increasing the irreversibility ratio.

The variation of average entropy generation rates and Bejan numbers with internal heat generation for the certain Rayleigh numbers is compared in Fig. 11 for the selected geometries. The average entropy generation rate consists of irreversibility due to heat, porous medium, fluid friction, both species and their couplings (Eq. (14)) and depends upon several pertinent parameters. In the absence of internal heat generation, the average entropy generation rate is found to be minimum and increases with increasing the heat

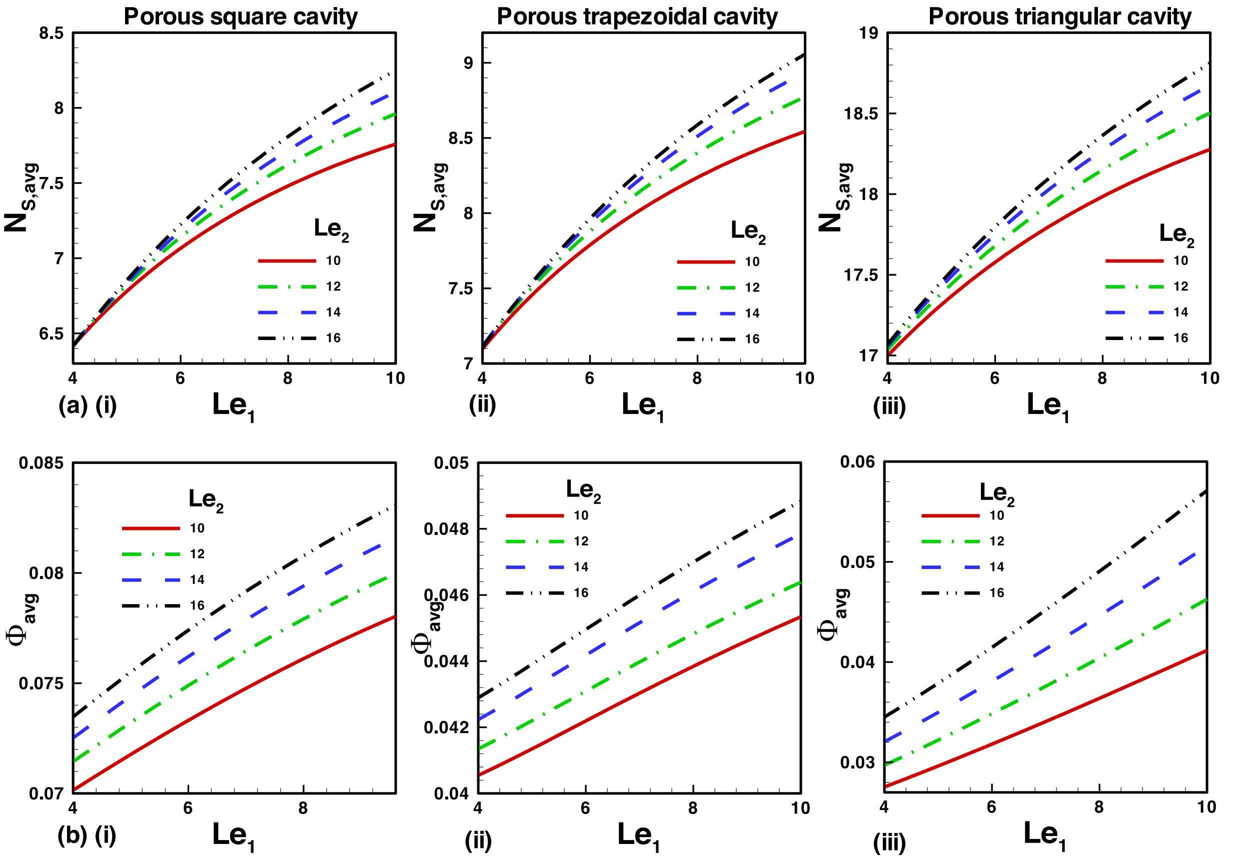

Fig. 10. Effects of Lewis numbers on average entropy generation rate and average irreversibility ratio for different cavities with$Ra = 50, Da = 10^{-4}$, $\varphi_1 = \varphi_2 = 10^{-2}, \varphi_3 = 10^{-1}, Q = Nc_1 = Nc_2 = \varphi_4 = 0.5$.

generation. This is due to the increase in the heat transfer irreversibility, Fig. 11(a) (i)–(iii) illustrates this behavior within the selected cavities. Rayleigh number helps in enhancing natural convection and increases the total average entropy generation rate, as shown in Fig. 11(a) (iii). The comparison shows that the triangular cavity provides highest entropy generation rate than square and trapezoidal cavities.

By definition, the conventional Bejan number (Be_h) shows the share of the thermal irreversibility in the total entropy generation rate. The effects of Ra and heat generation parameter Q on Be_h are displayed in Fig. 11(b) (i)–(iii) for the selected cavities. In each case, $Be_h < 0.5$, which reveals that the thermal irreversibility is less than the irreversibility due to other sources. Due to increase in Ra, the buoyancy forces increase and as a result fluid flow irreversibility rises. Further Darcy number, due to porous medium, encourages the entropy generation. Consequently, the irreversibility due to other sources becomes higher than thermal irreversibility and the conventional Bejan number remains less than 0.5 in each case, as shown in Fig. 11(b) (i)–(iii). Like Ns, the Bejan number increases with internal heat generation and Ra in each cavity. The square cavity shows higher Bejan number than other cavities. Similar to conventional Bejan number, another type of mass Bejan number is defined in Eq. (21) which shows the contribution of the irreversibility due to different species with their coupling $(N_{S,C} = N_{S,C_1} + N_{S,C_2} + N_{S,C_{12}})$ in the total entropy generation rate N_S. The impacts of the heat generation parameter and Rayleigh number on the average mass Bejan number are illustrated in Fig. 11 (c) (i)–(iii) for each cavity. It is observed that, in each case, $Be_{mass} < 0.5$ which shows that the entropy generation rate is higher due to sources other than solutes, i. e.$N_{S,C} > N_{S,\text{othersources}}$ where $N_{S,\text{othersources}} = N_{s,h} + N_{s,f} + N_{s,pm}$.

Fig. 12(a) and (b) explains the variation of average heat and mass Bejan numbers with the buoyancy ratios in the selected geometries. The average heat Bejan number depends upon the thermal irreversibility which decreases with an increase in both buoyancy ratios. Consequently, the ratio $\frac{N_{S,\text{othersources}}}{N_{S,h}}$ increases and the average heat Bejan number decreases in each case (see Fig. 12(a) (i)-(iii)). For small buoyancy ratios, the contribution of thermal and other sources is found to be almost the same. As the buoyancy ratios increase, the dominance of irreversibility due to other sources upsurges. The comparison shows that the square cavity provides higher thermal irreversibility than other cavities. Fig. 12(b) represents the variation of average mass Bejan number $Be_{m,avg}$ with both buoyancy ratios for the selected geometries. In case of mass transfer, $N_{S,C}$ plays the same role as $N_{S,C}$ in heat transfer. $Be_{m,avg}$ depends upon irreversibility due to solutes and their coupling. $Be_{h,avg}$, $Be_{m,avg}$ are also decreased with both buoyancy ratios.

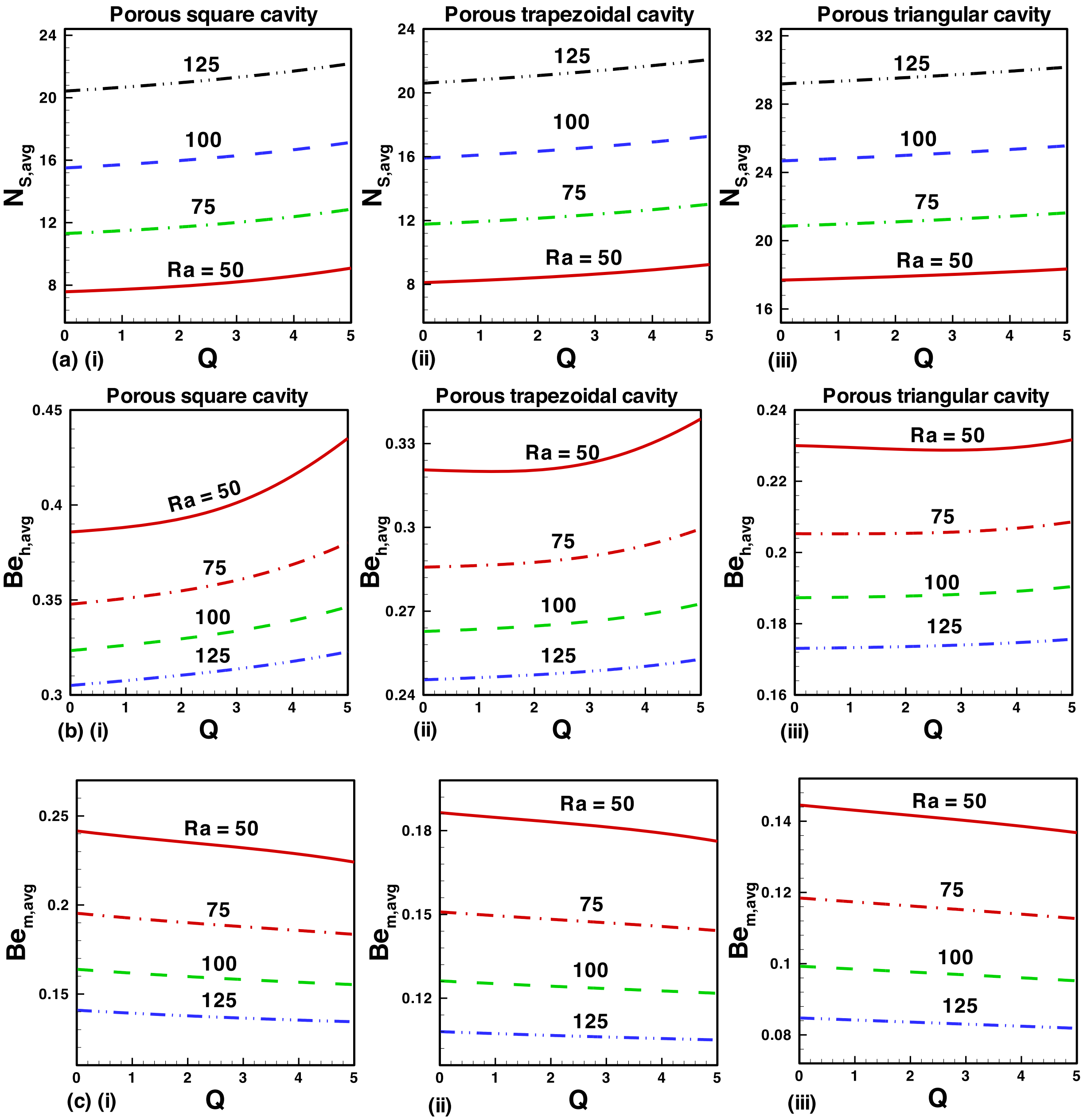

Fig. 11. Effects of heat generation parameter and Rayleigh number on (a) total average entropy generation rate (b) average heat Bejan number (c) average mass Bejan number for different cavities with $Le_1 = 8, Le_2 = 5, Da = 10^{-4}, \varphi_1 = \varphi_2 = 10^{-2}, \varphi_3 = 10^{-1}, Nc_1 = Nc_2 = \varphi_4 = 0.5$.

6. Conclusions

The entropy generation due to several sources in a triple-diffusive natural convection system of non-isothermal flows is analyzed. Effects of various governing parameters have been studied highlighting an influence of each irreversibility source on entropy generation. The summary of results is given below:

- Both internal heat generation and Rayleigh number tend to increase average entropy generation rate and Bejan number. Moreover, a rise of the Rayleigh number from 50 till 100 allows to double the average entropy generation for square and trapezoidal porous cavities, while for the triangular porous cavity such augmentation of the Rayleigh number allows to increase the average entropy generation rate in one and a half times.
- The square and trapezoidal cavities offer less entropy generation rate and higher Bejan number that can be useful for the engineering systems where the minimization of the entropy generation is desirable.

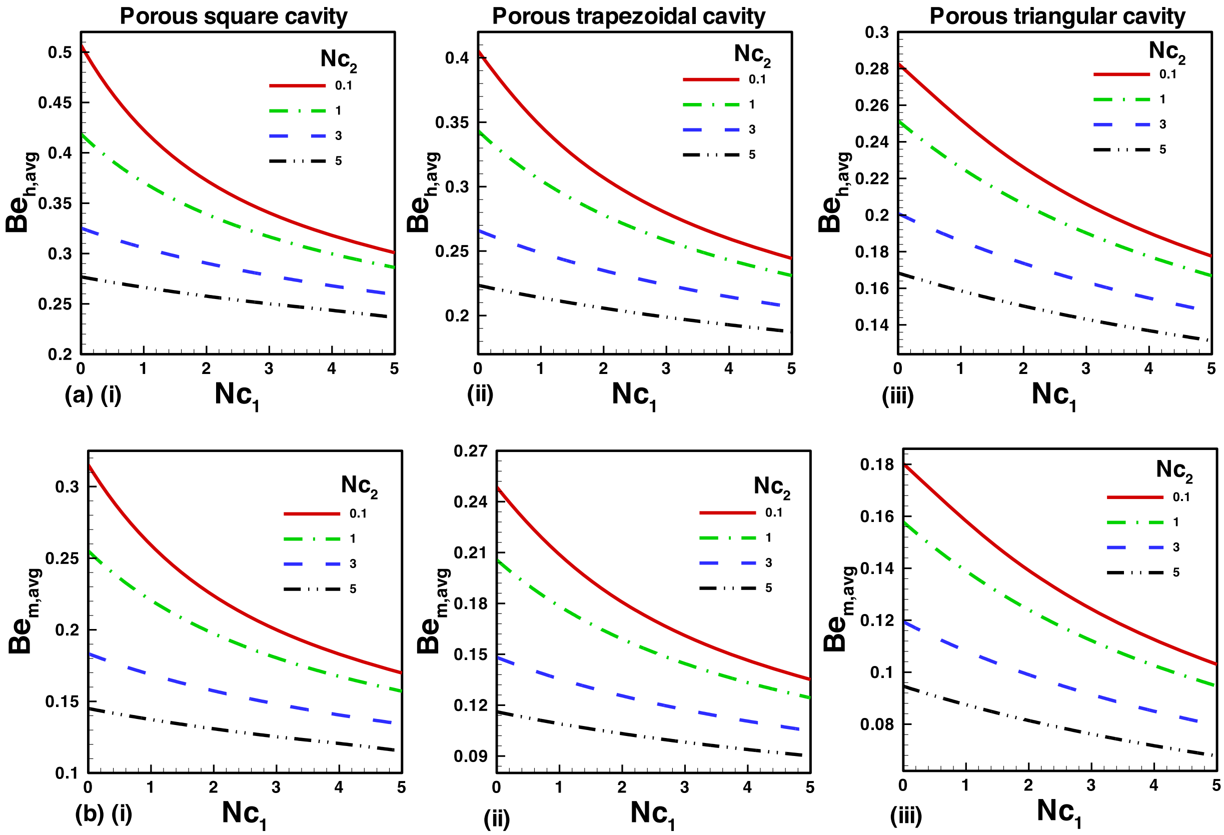

Fig. 12. Effects of buoyance ratios on (a) average heat Bejan number (b) average mass Bejan number for different cavities with $Ra = 50, Le_1 = 8, Le_2 = 5, Da = 10^{-4}, Q = \varphi_1 = \varphi_2 = \varphi_3 = \varphi_4 = 0.5$.

- Both internal heat generation and Rayleigh number tend to decrease the average mass Bejan number. Moreover, it is possible to reduce the average mass Bejan number up to one and a half times with a growth of Rayleigh number from 50 till 100 for each considered geometry of the porous cavity.
- The square cavity shows higher average mass Bejan number that characterizes less essential influence irreversibility due to heat transfer, porous medium and fluid friction on mass transfer in the square porous cavity.
- Lewis numbers tend to increase the average total entropy generation rate and irreversibility ratio. By the way, an essential influence of Le_2 can be found for high values of Le_1.
- Both average heat and mass Bejan numbers decrease with an increase in the buoyancy ratios of both salts.
- The average entropy generation rate and irreversibility ratio increase with an increase in the buoyancy ratios. Moreover, a growth of the average entropy generation rate up to four times can be achieved with Nc_2 for low value of Nc_1 in the case of square and trapezoidal chambers.
- Local entropy generation is observed on the upper corner of the cooled side and lower corner of the heated side of the cavity.

Availability of data Statement

The datasets generated and analyzed during the current study are available from the corresponding author on reasonable request.

Declaration of Competing Interest

All the authors declare no actual or potential conflict of interest, including any financial, personal, or other relationships with other people or organizations.

Acknowledgment

The first author is profoundly grateful to the financial support of the Thousand Talents Plan 2019 “for the Introduction of High-level Talents at Home and Abroad in Sichuan Province”. The corresponding authors (J. Tang) and L. Sun are grateful to the financial support of the National Natural Science Foundation of China (Grant Nos 52076144 and 12075160) and Sichuan Science and Technology

Program (Grant No. 2021YJ0374). The third author Mikhail A. Sheremet is profoundly grateful to the financial support of the Ministry of Science and Higher Education of the Russian Federation (Project Number 0721-2020-0036) .

References

[1] A. Bejan, Entropy Generation Through Heat and Fluid Flow, Wiley, 1982.
[2] A. Bejan, Entropy Generation Minimization: The Method of Thermodynamic Optimization of Finite-Size Systems and Finite-Time Processes, CRC Press, 1995.
[3] A. Bejan, Advanced Engineering Thermodynamics, 4th Edition, Wiley, 2016.
[4] L. Virto, M. Carbonell, R. Castilla, P.J. Gamez-Montero, Heating of saturated porous media in practice: several causes of local thermal non-equilibrium, Int. J. Heat Mass Transf. 52 (2009) 5412–5422.
[5] S. Rashidi, J.A. Esfahani, N. Karimi, Porous materials in building energy technologies – a review of the applications, modelling and experiments, Renew. Sustain. Energy Rev. 91 (2018) 229–247.
[6] M. Torabi, N. Karimi, G.P. Peterson, S. Yee, Challenges and progress on the modelling of entropy generation in porous media: a review, Int. J. Heat Mass Transf. 114 (2017) 31–46.
[7] A. Bairi, Using nanofluid saturated porous media to enhance free convective heat transfer around a spherical electronic device, Chin. J. Phys. 70 (2021) 106–116.
[8] W.C. Tan, L.H. Saw, H.S. Thiam, J. Xuan, Z. Cai, M.C. Yew, Overview of porous media/metal foam application in fuel cells and solar power systems, Renew. Sustain. Energy Rev. 96 (2018) 181–197.
[9] T. Wan, Y. Liu, C. Zhou, X. Chen, Y. Li, Fabrication, properties, and applications of open-cell aluminum foams: a review, J. Mater. Sci. Technol. 62 (2021) 11–24.
[10] S. Rashidi, M.H. Kashefi, K.C. Kim, O. Samimi-Abianeh, Potentials of porous materials for energy management in heat exchangers – a comprehensive review, Appl. Energy 243 (2019) 206–232.
[11] A.M. Siddiqui, Q.A. Azim, Creeping flow of a viscous fluid in a uniformly porous slit with porous medium: an application to the diseased renal tubules, Chin. J. Phys. 64 (2020) 264–277.
[12] A.I. Alsabery, T. Tayebi, A.J. Chamkha, I. Hashim, Effect of rotating solid cylinder on entropy generation and convective heat transfer in a wavy porous cavity heated from below, Int. Commun. Heat Mass Transf. 95 (2018) 197–209.
[13] P. Biswal, A. Nag, T. Basak, Analysis of thermal management during natural convection within porous tilted square cavities via heatline and entropy generation, Int. J. Mech. Sci. 115-116 (2016) 596–615.
[14] R.S. Kaluri, T. Basak, Role of entropy generation on thermal management during natural convection in porous square cavities with distributed heat sources, Chem. Eng. Sci. 66 (2011) 2124–2140.
[15] D. Ramakrishna, T. Basak, S. Roy, E. Momoniat, Analysis of thermal efficiency via analysis of heat flow and entropy generation during natural convection within porous trapezoidal cavities, Int. J. Heat Mass Transf. 77 (2014) 98–113.
[16] T. Basak, P. Gunda, R. Anandalakshmi, Analysis of entropy generation during natural convection in porous right-angled triangular cavities with various thermal boundary conditions, Int. J. Heat Mass Transf. 55 (2012) 4521–4535.
[17] A.C. Baytas, Entropy generation for natural convection in an inclined porous cavity, Int. J. Heat Mass Transf. 43 (2000) 2089–2099.
[18] M.A. Vatanparast, S. Hossainpour, A. Keyhani-Asl, S. Forouzi, Numerical investigation of total entropy generation in a rectangular channel with staggered semi-porous fins, Int. Commun. Heat Mass Transf. 111 (2020), 104446.
[19] A.M. Rashad, T. Armaghani, A.J. Chamkha, M.A. Mansour, Entropy generation and MHD natural convection of a nanofluid in an inclined square porous cavity: Effects of a heat sink and source size and location, Chin. J. Phys. 56 (2018) 193–211.
[20] M. Siavashi, R. Yousofvand, S. Rezanejad, Nanofluid and porous fins effect on natural convection and entropy generation of flow inside a cavity, Adv. Powder Technol. 29 (2018) 142–156.
[21] S.H. Hussain, Analysis of heatlines and entropy generation during double-diffusive MHD natural convection within a tilted sinusoidal corrugated porous enclosure, Eng. Sci. Technol. Int. J. 19 (2) (2016) 926–945.
[22] T. Tayebi, H.F. Oztop, J. A., Chamkha Natural convection and entropy production in hybrid nanofluid filled-annular elliptical cavity with internal heat generation or absorption, Therm. Sci. Eng. Progr. 19 (2020), 100605.
[23] N.S. Gibanov, M.A. Sheremet, H.F. Oztop, K. Al-Salem, Effect of uniform inclined magnetic field on natural convection and entropy generation in an open cavity having a horizontal porous layer saturated with a ferrofluid, Numer. Heat Transf. A 72 (6) (2017) 479–494.
[24] A.J. Chamkha, I.V. Miroshnichenko, M.A. Sheremet, Unsteady conjugate natural convective heat transfer and entropy generation in a porous semi-circular cavity, J. Heat Transf. 140 (6) (2018), 062501.
[25] N.S. Gibanov, M.A. Sheremet, H.F. Oztop, K. Al-Salem, MHD natural convection and entropy generation in an open cavity having different horizontal porous blocks saturated with a ferrofluid, J. Magn. Magn. Mater. 452 (2018) 193–204.
[26] G.S. Seth, A. Bhattacharyya, R. Kumar, A.J. Chamkha, Entropy generation in hydromagnetic nanofluid flow over a non-linear stretching sheet with Navier's velocity slip and convective heat transfer, Phys. Fluids 30 (2018), 122003.
[27] Y.-X. Li, M.I. Khan, R.J.P. Gowda, A. Ali, S. Farooq, Y.-M. Chu, S.U. Khan, Dynamics of aluminum oxide and copper hybrid nanofluid in nonlinear mixed Marangoni convective flow with entropy generation: applications to renewable energy, Chin. J. Phys. (2021) 10.1016/j.cjph.2021.06.004.
[28] F. Arpino, N. Massarotti, A. Mauro, A stable explicit fractional step procedure for the solution of heat and fluid flow through interfaces between saturated porous media and free fluids in presence of high source terms, Int. J. Numer. Methods Eng. 83 (6) (2010) 671–692.
[29] A.C. Baytas, A.F. Baytas, D.B. Ingham, I. Pop, Double diffusive natural convection in an enclosure filled with a step type porous layer: Non-Darcy flow, Int. J. Therm. Sci. 48 (4) (2009) 665–673.
[30] N. Massarotti, M. Ciccolella, G. Cortellessa, A. Mauro, New benchmark solutions for transient natural convection in partially porous annuli, Int. J. Numer. Methods Heat Fluid Flow 26 (3/4) (2016) 1187–1225.
[31] D.V.K. Prasad, G.S.K. Chaitanya, R.S. Raju, Double diffusive effects on mixed convection Casson fluid flow past a wavy inclined plate in presence of Darcian porous medium, Results Eng. 3 (2019), 100019.
[32] B. He, S. Lu, D. Gao, W. Chen, F. Lin, Lattice Boltzmann simulation of double diffusive natural convection in heterogeneously porous media of a fluid with temperature-dependent viscosity, Chin. J. Phys. 63 (2020) 186–200.
[33] F. Arpino, N. Massarotti, A. Mauro, P. Nithiarasu, Artificial compressibility based CBS solutions for double diffusive natural convection in cavities, Int. J. Numer. Methods Heat Fluid Flow 23 (1) (2013) 205–225.
[34] P.M. Patil, M. Roy, A. Shashikant, S. Roy, E. Momoniat, Triple diffusive mixed convection from an exponentially decreasing mainstream velocity, Int. J. Heat Mass Transf. 124 (2018) 298–306.
[35] G.S. Seth, R. Kumar, R. Tripathi, A. Bhattacharyya, Double diffusive MHD Casson fluid flow in a non-Darcy porous medium with Newtonian heating and thermo-diffusion effects, Int. J. Heat Technol. 36 (4) (2018) 1517–1527.
[36] A. Bhattacharyya, R. Kumar, G.S. Seth, Capturing the features of peristaltic transport of a chemically reacting couple stress fluid through an inclined asymmetric channel with Dufour and Soret effects in presence of inclined magnetic field, Indian J. Phys. (2021) 10.1007/s12648-020-01936-8.
[37] A. Bhattacharyya, G.S. Seth, R. Kumar, Modeling of viscoelastic fluid flow past a non-linearly stretching surface with convective heat transfer: OHAM analysis, in: Proceedings of the ICMMSC 308, 2018, pp. 297–312. Mathematical Modelling and Scientific Computing with Applications.
[38] J.C. Umavathi, O.A. Beg, Modeling the onset of thermosolutal convective instability in a non-Newtonian nanofluid-saturated porous medium layer, Chin. J. Phys. 68 (2020) 147–167.
[39] M.A. Mansour, S.E. Ahmed, A.M. Aly, Z.A.S. Raizah, Triple convective flow of micropolar nanofluids in double lid-driven enclosures partially filled with LTNE porous layer under effects of an inclined magnetic field, Chin. J. Phys. 68 (2020) 387–405.

[40] A. Mchirgui, N. Hidouri, M. Magherbi, A.B. Brahim, Entropy generation in double-diffusive convection in a square porous cavity using Darcy–Brinkman formulation, Transp. Porous Media 93 (1) (2012) 223–240.
[41] A. Mchirgui, N. Hidouri, M. Magherbi, A.B. Brahim, Second law analysis in double diffusive convection through an inclined porous cavity, Comput. Fluids 96 (2014) 105–115.
[42] GH.R. Kefayati, Simulation of double diffusive natural convection and entropy generation of power-law fluids in an inclined porous cavity with Soret and Dufour effects (Part I: Study of fluid flow, heat and mass transfer), Int. J. Heat Mass Transf. 94 (2016) 539–581.
[43] GH.R. Kefayati, Simulation of double diffusive natural convection and entropy generation of power-law fluids in an inclined porous cavity with Soret and Dufour effects (Part II: Entropy generation), Int. J. Heat Mass Transf. 94 (2016) 582–624.
[44] M. Siavashi, V. Bordbar, P. Rahnama, Heat transfer and entropy generation study of non-Darcy double-diffusive natural convection in inclined porous enclosures with different source configurations, Appl. Therm. Eng. 110 (2017) 1462–1475.
[45] Q.Y. Zhu, Y.J. Zhuang, H.Z. Yu, Entropy generation due to three-dimensional double-diffusive convection of power-law fluids in heterogeneous porous media, Int. J. Heat Mass Transf. 106 (2017) 61–82.
[46] S. Hussain, K. Mehmood, M. Sagheer, M. Yamin, Numerical simulation of double diffusive mixed convective nanofluid flow and entropy generation in a square porous enclosure, Int. J. Heat Mass Transf. 122 (2018) 1283–1297.
[47] Z.H. Khan, W.A. Khan, M.A. Sheremet, Enhancement of heat and mass transfer rates through various porous cavities for triple convective-diffusive free convection, Energy 201 (2020), 117702.
[48] S. Rionero, Triple diffusive convection in porous media, Acta Mech. 224 (2013) 447–458.
[49] D.A. Nield, A. Bejan, Convection in Porous Media, Springer, 2013.
[50] Z.H. Khan, W.A. Khan, J. Tang, M.A. Sheremet, Entropy generation analysis of triple diffusive flow past a horizontal plate in porous medium, Chem. Eng. Sci. 228 (2020), 115980.
[51] G.G. Ilis, M. Mobedi, B. Sunden, Effect of aspect ratio on entropy generation in a rectangular cavity with differentially heated vertical walls, Int. Commun. Heat Mass Transf. 35 (2008) 696–703.
[52] S. Bhardwaj, A. Dalal, S. Pati, Influence of wavy wall and non-uniform heating on natural convection heat transfer and entropy generation inside porous complex enclosure, Energy 79 (2015) 467–481.